




# High permittivity ceramics-filled acrylonitrile butadiene rubber composites: influence of acrylonitrile content and ceramic type

Piyawadee Luangchuang<sup>1</sup> · Narong Chueangchayaphan<sup>1</sup> · Muhammad Azwadi Sulaiman<sup>2</sup> · Wannarat Chueangchayaphan<sup>1</sup> 

Received: 27 November 2019 / Revised: 3 March 2020 / Accepted: 19 March 2020 /  
Published online: 1 April 2020  
© Springer-Verlag GmbH Germany, part of Springer Nature 2020

## Abstract

Influence of acrylonitrile content and ceramic type on cure characteristics, mechanical, morphological, and dielectric properties of acrylonitrile butadiene rubber (NBR) vulcanizates was examined. Two types of ceramic filler, namely barium titanate (BT) and calcium copper titanate (CCTO), were synthesized by solid-state reactions. The ceramic powders were then characterized by X-ray diffraction, particle size analyzer, and scanning electron microscopy (SEM). Ceramic/rubber composites were then mixed in an internal mixer at 60 °C and a rotor speed of 60 rpm. Two acrylonitrile contents of NBR, namely 33 wt% and 42 wt%, were tested. Incorporation of ceramic fillers in NBR matrix and increasing acrylonitrile content shortened scorch and cure times, but increased minimum, maximum, and delta torque. Furthermore, SEM results revealed that the BT-filled NBR composites showed better filler–matrix interactions than the CCTO-filled NBR composites. This matches the better mechanical and dielectric properties of the BT-filled NBR composites.

**Keywords** Acrylonitrile butadiene rubber · Acrylonitrile content · Barium titanate · Dielectric properties · Calcium copper titanate · Mechanical properties

## Introduction

Nowadays, polymers have been developed a variety of different compounds with unique potential for various applications, i.e., membrane for wastewater treatment [1–4], pH-stimulated micellization for drug delivery [5], shape memory polymer

---

✉ Wannarat Chueangchayaphan  
wannarat.p@psu.ac.th

<sup>1</sup> Faculty of Science and Industrial Technology, Prince of Songkla University, Surat Thani Campus, Surat Thani 84000, Thailand

<sup>2</sup> Advanced Materials Research Cluster, Faculty Bioengineering and Technology, Universiti Malaysia Kelantan, 17600 Jeli, Kelantan, Malaysia

[6–7], and self-healing polymer [8]. In particular, high permittivity ceramics-filled polymer composites are motivated by potential electrical and electronics applications, such as energy storage capacitors, actuators, and smart packaging technology, due to their light weight, flexibility, acceptable dielectric properties, and easy processing [9–11]. Among the choices of polymer matrix, nitrile rubber or acrylonitrile butadiene rubber (NBR) has received attention because it contains acrylonitrile groups ( $C\equiv N$ ) that contribute by orientation polarization [12]. NBR is a family of elastomers obtained by the random co-polymerization of acrylonitrile and butadiene. It has an extensive variety of grades dependent on acrylonitrile content and has excellent oil resistance over a wide range of temperatures [13], excellent abrasion resistance, low compression set, good heat resistance, and high tensile properties when suitably compounded. The polar acrylonitrile group also affects the glass transition temperature ( $T_g$ ) and hence the entropy elastic behavior [14]. However, poor properties in elasticity, low temperature resistance, and poor insulation capacity tend to go with increasing acrylonitrile content [12]. In addition, NBR does not exhibit self-reinforcement effect [13, 15], which is usually attributed to its uniform microstructure with crystallites acting as additional crosslinks in the network structure, and these tend to align in the direction of stretching [16]. Hence, excellent mechanical properties are only obtained by combinations with reinforcing fillers. Carbon black [17], clay [18–20], silica [21, 22], graphene oxide [23, 24], carbon nanotubes [24], and carbon nanofibers [25] have been tested in NBR matrix. However, there are hardly any reports on adding a high permittivity ceramic to NBR rubber. Among the ceramic fillers, barium titanate (BT) and copper calcium titanate (CCTO) have been much investigated in polymer composites [26–46].

The present study is motivated by the need to develop flexible dielectric materials. NBR with different acrylonitrile contents was chosen as the polymer matrix to prepare composites with different ceramic fillers, here barium titanate (BT) and calcium copper titanate (CCTO). X-ray diffraction (XRD), particle size analysis, and scanning electron microscopy (SEM) were used to characterize the ceramic fillers. The effects of acrylonitrile content and ceramic type on cure characteristics, mechanical, dynamic mechanical, thermal, morphological, and dielectric properties of NBR/ceramic composites were evaluated.

## Experimental

### Materials

The ceramic fillers, BT and CCTO, were synthesized by conventional solid-state reactions. The reagent-grade high-purity calcium carbonate ( $CaCO_3$ ), copper (II) oxide (CuO), and titanium dioxide ( $TiO_2$ ) used as starting materials were supplied by LabChem public Co., Ltd. (Surat Thani, Thailand). The acrylonitrile butadiene rubber (NBR) with 33% and 42% acrylonitrile contents was received from Nantex public Co., Ltd. (Kaohsiung 832, Taiwan). 2-Mercaptobenzothiazyl disulfide (MBTs) and sulfur were provided by Vessel chemical public Co., Ltd. (Bangkok, Thailand). Zinc oxide (ZnO) and stearic acid were obtained from Bossoftical public

**Table 1** Compounding formulations

Ingredient/compound	Amount (phr)			
	N33	N33B	N33C	N42C
NBR 33% acrylonitrile content	100	100	100	–
NBR 42% acrylonitrile content	–	–	–	100
Sulfur	1.5	1.5	1.5	1.5
Zinc oxide	5	5	5	5
Stearic acid	2	2	2	2
MBTs	1.5	1.5	1.5	1.5
BT	–	60	–	–
CCTO	–	–	60	60

**Table 2** Details of the materials and mixture schedule

Mixing procedure	Function	
Internal mixer	Cumulative time (min)	
Mastication of NBR	0	Main matrix
Addition of sulfur	2	Curing agent
Addition of ZnO	4	Activator
Addition of stearic acid	6	Activator
Addition of ceramic filler	7	Filler
Addition of MBTS	10	Accelerator
Dumping	12	

Co., Ltd. (Songkhla, Thailand). All substances were used as received without further purification.

**Characterization of ceramic fillers**

X-ray diffraction (XRD) was operated at 40 kV, 30 mA, from 10° to 90° (2θ) with Cu-Kα radiation, and the device was equipped with a 0.154 monochromator. Particle size analysis and SEM imaging were used to assess the particle sizes and morphologies of the ceramic fillers.

**Preparation and characterization of NBR/ceramic composites**

NBR/ceramic composites were melt mixed in an internal mixer at 60 °C with 60 rpm rotor speed. The compounding formulation and procedure are listed in Tables 1 and 2. The rubber compounds were sheeted out on a two roll mill after compounding in an internal mixer and were kept in a desiccator for 24 h at room temperature before vulcanizing and testing. 2-mm-thick rubber composite sheets were hydraulically compression molded at 160 °C for the respective cure times,  $t_{c90}$ , determined

by MDR test. The moving die rheometer (MDR) was used to determine minimum torque ( $M_L$ ) and maximum torque ( $M_H$ ), torque difference ( $M_H - M_L$ ), scorch time ( $t_{s1}$ ), and cure time ( $t_{c90}$ ) of virgin NBR and its compounds. The measurements were performed at 160 °C according to ASTM2240 at a fixed oscillation frequency of 1.66 Hz with 1 arc degree amplitude.

The tensile strength, elongation at break, 100% modulus, and 300% modulus were obtained from tensile testing according to ASTM D-412. The tests were carried out at  $23 \pm 2$  °C, using a 500 mm/min cross-head speed. Also, 6-mm-thick samples were Hardness Shore A tested according to ASTM D2240 with a durometer. Thermogravimetric analysis (TGA) was carried out with a simultaneous thermal analyzer with a heating rate of 10 °C/min in the temperature range from 25 to 1000 °C. The samples were tested in nitrogen atmosphere in the early stage, with switch to oxygen atmosphere when the temperature passed 550 °C. A PerkinElmer DMTA 8000 was used for dynamic mechanical thermal analysis. The samples were tested in tension mode from  $-100$  to 50 °C at a heating rate of 3 °C/min, with frequency and strain fixed at 10 Hz and 0.1%, respectively. The dielectric constant ( $\epsilon'$ ) and dielectric loss ( $\epsilon''$ ) were measured using an impedance analyzer in the frequency range  $10^5$ – $10^7$  Hz at AC potential of 1 V. The samples were placed between two parallel plate electrodes of 5 mm diameter and tested at room temperature. The morphology of the composites was determined by scanning electron microscopy (SEM) (FEI-Quanta 400, OR, USA). The samples were first cryogenically fractured after immersion in liquid nitrogen and were then sputter coated with gold before imaging.

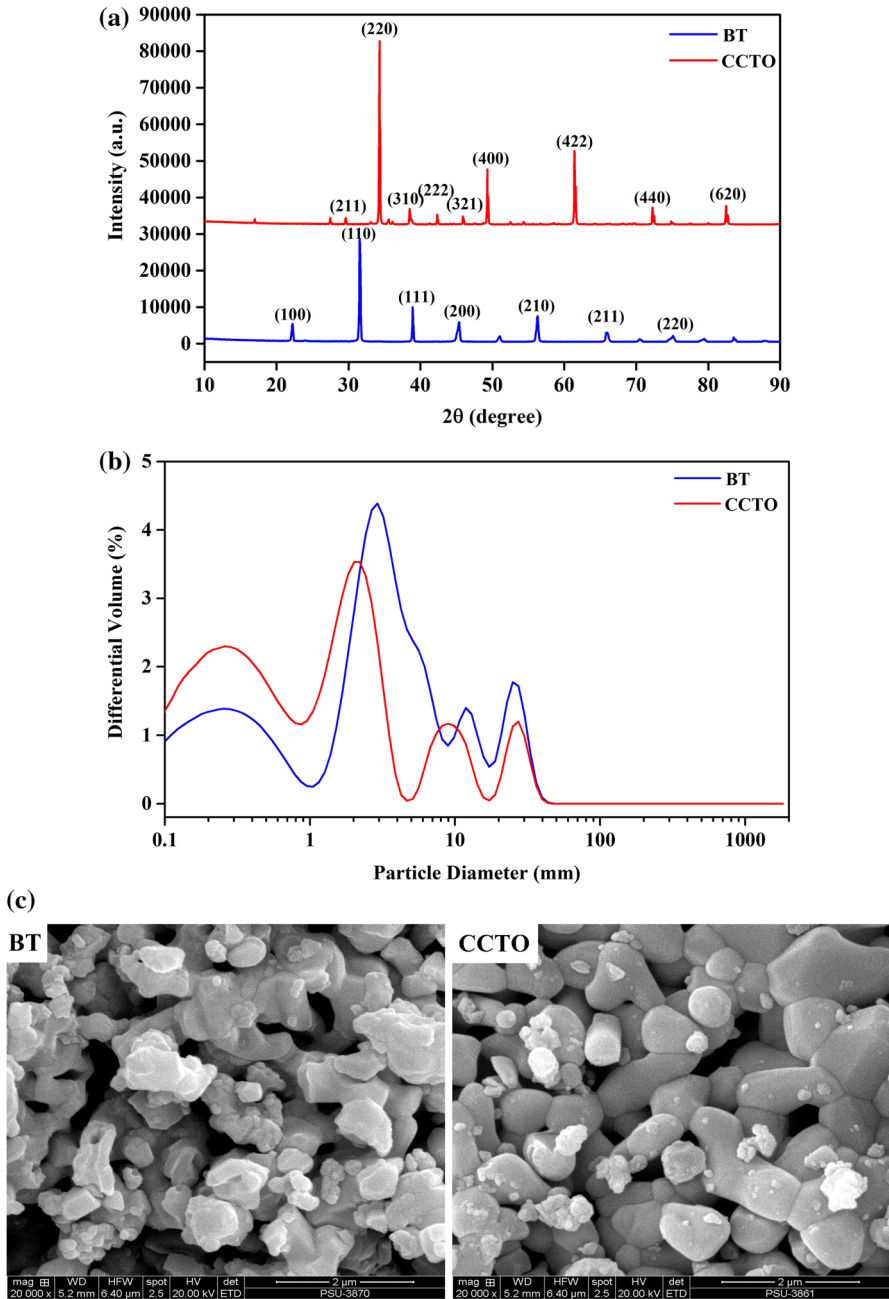
## Results and discussion

### Characterization of ceramic fillers

Figure 1a shows XRD patterns of BT and CCTO ceramic fillers. The structure of BT was characterized by XRD peaks at  $2\theta$  of 21.5°, 31.5°, 38.9°, 45.4°, 50.9°, 56.1°, and 66.1° corresponding to the (100), (110), (111), (200), (210), (211), and (220) planes. The XRD pattern of CCTO had peaks at 29.60°, 34.49°, 38.54°, 42.44°, 45.97°, 49.2°, 61.4°, 72.2°, and 82.56°, which were assigned to the lattice planes (211), (220), (310), (222), (321), (400), (422), (420), and (620), respectively. These results confirmed BT and CCTO crystal structures. Additional quantitative information of the particle size distributions of BT and CCTO is exhibited in Fig. 1b. The particle size of BT was larger than that of CCTO, with mass-average particle sizes approximately 5.56 and 3.41  $\mu\text{m}$ , respectively. Irregular shapes were noted for both CCTO and BT particles, as seen in Fig. 1c.

### Cure characteristics of composites

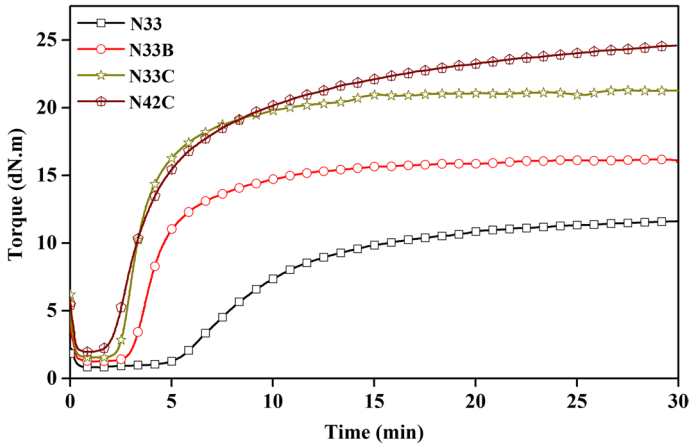
Cure characteristics of the virgin NBR and the NBR/ceramic composites in terms of scorch time, cure time, and minimum, maximum, and delta torques are listed in Table 3. The vulcanization curves of all samples are shown in Fig. 2. All the



**Fig. 1** a XRD patterns, b particle size distribution, and c SEM micrographs of BT and CCTO particles

**Table 3** Cure characteristics of virgin NBR and NBR/ceramic composites

Sample	$M_L$ (dN m)	$M_H$ (dN m)	$M_H - M_L$ (dN m)	$t_{s1}$ (min)	$t_{c90}$ (min)	CRI
N33	0.81	11.61	10.80	6.21	18.23	8.31
N33B	1.65	16.18	16.49	2.18	15.06	7.76
N33C	1.68	21.29	19.61	2.23	13.28	9.04
N42C	1.96	24.60	22.64	2.05	15.51	7.43

**Fig. 2** Cure curves of virgin NBR and NBR/ceramic composites

samples exhibited marching cure, so that the modulus kept increasing with time. This is attributed to the butadiene-containing polymers, with less polysulfidic bonds but rich in disulfidic and monosulfidic crosslinks with high crosslink density [47]. The marching characteristic was more pronounced for the N42C compounds, probably because the amount of double bonds in NBR rubber is limited. In addition, the acrylonitrile functional group ( $-C\equiv N$ ) might hinder the reactions between sulfur and the allylic radicals in butadiene units, at the higher acrylonitrile content resulting in a retard optimum cure time. However, the scorch time of N42C became faster as acrylonitrile content increased. Choi et al. explained that the polar acrylonitrile groups of NBR activated the zinc complexes resulting in the fast crosslink reaction [48]. In addition, Chokanandsombat et al. reported the effect of polar acrylonitrile groups on the decomposition of accelerators to produce ammonium mercaptide which acted as actual cure accelerator [49]. In addition,  $M_L$ ,  $M_H$  and  $M_H - M_L$  of N42C were higher than those of N33C. This is because an increase in acrylonitrile content gave a higher polarity, leading especially to greater rubber–rubber interactions, which limited molecular mobility. It is noted that increased acrylonitrile content also made the composite stiffer, because chemical and physical reactions among acrylonitrile groups produced high crosslinking level in NBR [50]. In addition, the NBR/ceramic composites had shorter cure and scorch times compared to N33. During compound mixing, the composites were subjected to shear during blending,

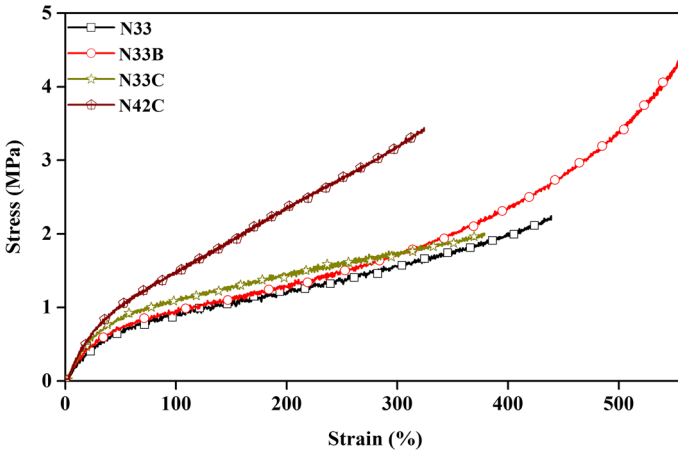


Fig. 3 Stress–strain behavior of virgin NBR and NBR/ceramic composites

Table 4 Mechanical properties of virgin NBR and NBR/ceramic composites

Sample	Tensile strength (MPa)	Elongation at break (%)	100% Modulus (MPa)	300% Modulus (MPa)	Hardness (shore A)
N33	2.15 ± 0.14	441 ± 3	0.87 ± 0.04	1.51 ± 0.04	42.1 ± 0.4
N33B	4.80 ± 0.14	561 ± 3	1.02 ± 0.04	1.63 ± 0.04	48.3 ± 0.3
N33C	1.95 ± 0.01	353 ± 3	1.69 ± 0.02	1.75 ± 0.03	51.4 ± 0.4
N42C	3.17 ± 0.03	251 ± 3	1.92 ± 0.01	2.02 ± 0.03	55.7 ± 0.3

generating heat. This heat induced premature curing [51]. N33C exhibited higher cure rate index than N33B. This indicates higher rate of vulcanization in the CCTO compounds. Moreover, the ceramic fillers tended to increase  $M_L$ ,  $M_H$  and  $M_H - M_L$  over that in N33. This might be attributed to increase filler–filler interactions and filler–rubber interactions. The torques seen in these curves were concordant with measured hardness.

### Mechanical properties

Stress–strain curves of the samples and mechanical properties are shown in Fig. 3 and in Table 4, respectively. It was found that N33, N33C, and N42C did not crystallize under stress, resulting in a low tensile strength. Furthermore, N33 exhibited the lowest Young’s modulus, 100% modulus, 300% modulus and hardness among the NBR/ceramic composites because the rigid ceramic particles in the soft matrix increased stiffness. This correlated with increased  $M_H$  and  $M_H - M_L$  as previously mentioned. With regard to the N33, 60 phr of BT incorporated into NBR caused a 125% increase in tensile strength. However, N33C gave tensile strength and

elongation at break below those of N33B and even lower than N33. Saidina et al. [37] reported a similar result in which the tensile properties of CCTO/epoxy composites were poorer than the corresponding values for BT/epoxy composites. This might be attributed to poor interactions between CCTO and NBR. This indicates that CCTO was a non-reinforcing filler, while BT served as a reinforcing filler. The reinforcing effect of N33B was due to good filler–rubber interactions via hydrogen bonding between acrylonitrile groups and hydrogen groups on BT particles [52, 53]. The N42C exhibited higher 100% modulus, 300% modulus, tensile strength, and hardness but lower elongation at break than the N33C. The hardness, 100% modulus, 300% modulus, and tensile strength were improved by 8.4%, 13.6%, 15.4%, and 62.5%, respectively, while elongation at break decreased by 28.9% on increasing acrylonitrile content. Yuan et al. showed similar results in which the tensile strength of  $\text{CuSO}_4/\text{NBR}$  composites increased noticeably with increasing acrylonitrile content [54]. This is attributed to stronger chemical interactions with NBR at a higher acrylonitrile content. This limited molecular mobility, increased stiffness, and decreased flexibility of the material.

### Morphology characterization

Figure 4 shows fractured sample surfaces. N33 displayed smoother surface than the NBR/ceramic composites. The dispersed ZnO particles were observed as white spots in N33. Inhomogeneous surfaces were observed for the NBR/ceramic

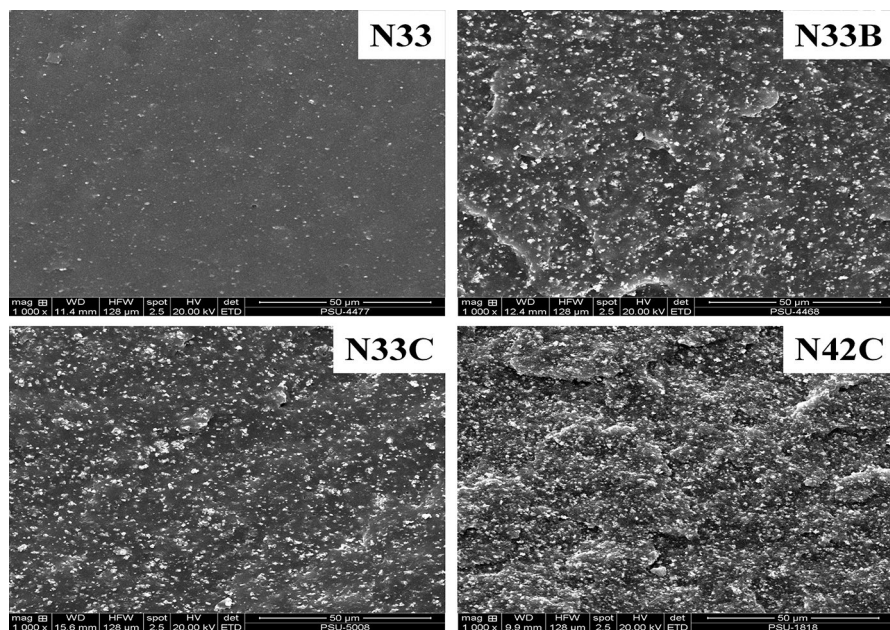


**Fig. 4** SEM images of fracture surfaces of virgin NBR and NBR/ceramic composites



composites. N33B exhibited rougher surface than N33C, indicating strong interactions of BT and NBR that improved the mechanical properties over those of N33C. The smoother surface of N33C implies poor interfacial compatibility, resulting in poor mechanical properties and poor dielectric constant compared with N33B. However, with increasing acrylonitrile content, apparently a rough surface of N42C was obtained. This is attributed to increased chemical interactions of the attached groups and side chains in NBR matrix, due to the polar groups in the elastomer.

### Dynamic mechanical analysis and thermal stability

Dynamic mechanical properties of virgin NBR and ceramics-filled composites are demonstrated in Fig. 5. In comparison with the virgin NBR sample, it can be seen that the storage modulus of N33B increased while the storage modulus of N33C decreased. Higher storage modulus indicates higher stiffness of a composite, due to strong interactions between BT and NBR. Though the storage modulus of N33B was increased, N33C had a reduced modulus due to the weak filler–rubber adhesion. However, with increasing acrylonitrile content, the storage modulus also increased. This is due to the strong intermolecular interactions of  $C\equiv N$  groups in NBR matrix at a high acrylonitrile content. These results agree well with the tensile properties. The glass transition temperatures of samples were obtained from the peak locations of  $\tan\delta$ . The  $T_g$  slightly shifted to higher temperatures for N33B and N33C, relative to N33. The  $T_g$  of N33 was at  $-20.6^\circ\text{C}$ . The incorporation of BT and CCTO slightly increased the  $T_g$  values to  $-19.6^\circ\text{C}$  and  $-19.0^\circ\text{C}$  for N33B and N33C, respectively. This indicates that ceramic particles obstructed the rubber chains, increasing  $T_g$ . Moreover, an increase in  $T_g$  was observed with increasing acrylonitrile content. The  $T_g$  of N42C was observed at  $-6.8^\circ\text{C}$  because of stronger chemical interactions among  $C\equiv N$  groups in NBR matrix that restricted mobility of rubber chains. Yuan et al. [54] and Song et al. [55] also reported a similar result in which

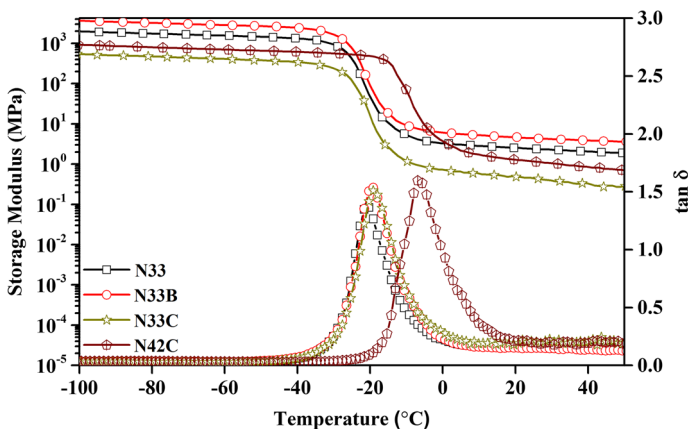


**Fig. 5** Storage modulus ( $E'$ ) and  $\tan\delta$  as functions of temperature for virgin NBR and NBR/ceramic composites

high acrylonitrile content gave a higher  $T_g$  than low acrylonitrile content. The results of TGA analysis on virgin NBR and ceramics-filled NBR composites with various ceramic types and acrylonitrile contents are shown in Fig. 6. It was found that the incorporation of ceramics into NBR matrix improved thermal stability of the composites, shifting the TGA curves toward higher temperatures. In addition, the NBR/ceramic composites displayed larger residual weights. This could be explained by the good thermal stability of the ceramic fillers themselves. There is no significant difference between N33C and N42C. This suggests a distinct improvement in the thermal stability of the NBR/ceramic composites by ceramic fillers, in this study.

### Dielectric properties of composites

Dielectric constant, dielectric loss, and conductivity as functions of frequency in the range from  $10^5$  to  $10^7$  Hz for all samples are shown in Fig. 7. The lowest dielectric constant was observed for N33. This was due to the intrinsic properties of the BT and CCTO ceramic fillers, which typically have higher dielectric constants than NBR. In comparison with N33, a 20% increase in dielectric constant of N33B at  $10^5$  Hz was obtained. However, N33C provided a lower dielectric constant than N33B. The dielectric constant of N33B was higher than N33C by 15% at  $10^5$  Hz. This is probably due to the poorer compatibility of CCTO with NBR matrix. However, it was found that N42C showed the lowest dielectric constant. The lower dielectric constant of N42C with higher acrylonitrile content compared with N33C was attributed to strong intermolecular interactions, which can limit orientation polarization [12]. Thipdech et al. found that the dielectric constant of virgin NBR increased with acrylonitrile content at frequencies below  $10^4$  Hz due to added  $C\equiv N$  dipoles, causing an increase in the orientation polymerization. However, NBR with 42.5% acrylonitrile content exhibited a larger drop in dielectric constant than the other cases with acrylonitrile contents of 42.5, 33, 28, and 18.5% when frequency exceeded  $10^4$  Hz [56]. Figure 7b presents the dielectric losses of the samples. A broad relaxation appeared at about  $10^6$  Hz because

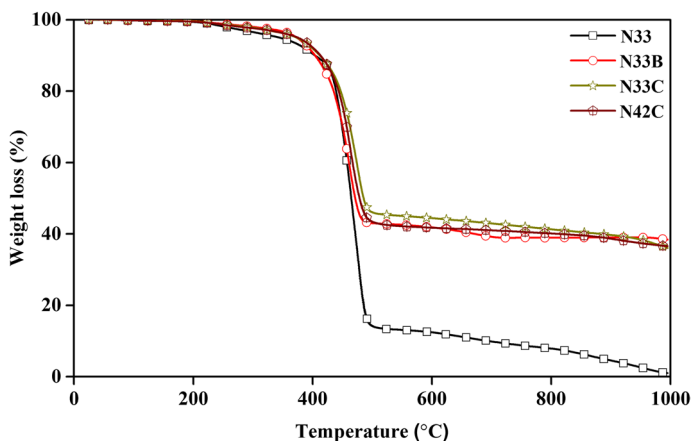
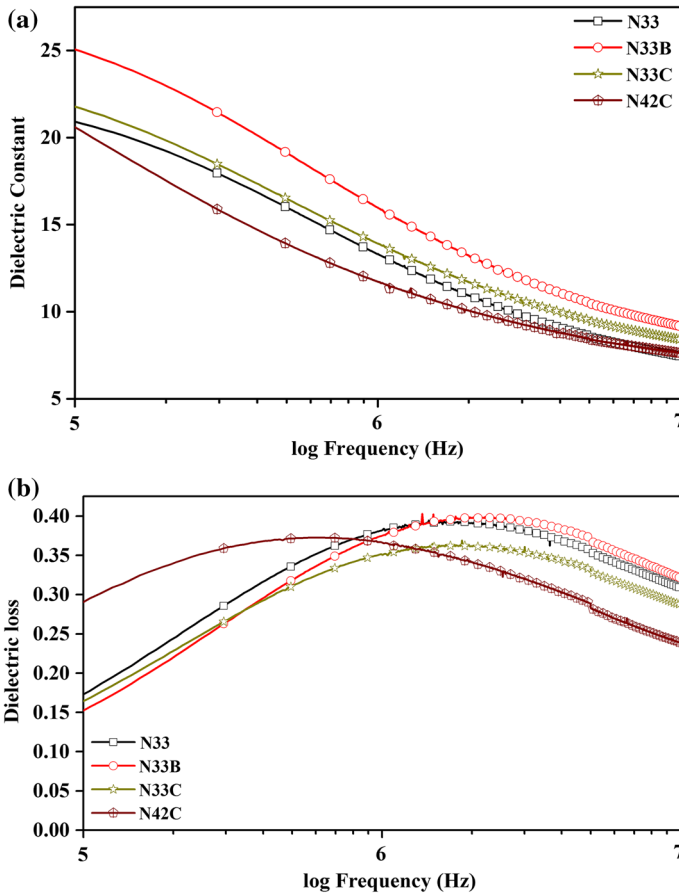


Fig. 6 TGA thermograms of virgin NBR and NBR/ceramic composites



**Fig. 7** **a** Dielectric constant and **b** dielectric loss of virgin NBR and NBR/ceramic composites

of the elastomer chain segmental motions [12, 57]. On incorporating ceramic fillers into NBR, there was no significant change in dielectric loss on adding BT, while there was a larger decrease in dielectric loss on adding CCTO and on increasing acrylonitrile content. The reduction in dielectric loss for ceramics-filled NBR was due to the fillers hindering C≡N dipole re-orientation [58]. This means that the ceramic fillers in NBR improved to some extent the insulating properties of NBR. In addition, a shift toward lower frequencies was observed on increasing acrylonitrile content, which may reflect resistance to C≡N dipole relaxation. As the acrylonitrile content increased, the stronger interactions between acrylonitrile groups hindered dipole re-orientation.

### Conclusions

The following conclusions can be drawn from this study:

1. Faster scorch and cure times as well as larger minimum, maximum, and delta torques were obtained on adding ceramic fillers into NBR matrix. The BT-filled NBR composite exhibited lower minimum, maximum, and delta torques and scorch time but higher cure time compared to the CCTO-filled NBR composite, while minimum, maximum, and delta torques and cure time increased but scorch time decreased with increasing acrylonitrile content.
2. BT-filled NBR composite exhibited a higher tensile strength of 4.80 MPa and elongation at break of 561% compared to virgin NBR or CCTO-filled NBR composite. In addition, 100% modulus, 300% modulus, tensile strength, and hardness increased, while elongation at break decreased with acrylonitrile content.
3. A rough surface was obtained with increasing acrylonitrile content and using BT as filler due to strong interactions of BT and NBR matrix
4. Higher  $T_g$  was observed after addition of ceramic fillers into NBR matrix and on increasing acrylonitrile content, from  $-20.6$  to  $-6.8$  °C. In addition, these ceramic fillers tested also improved thermal stability of the composites, but acrylonitrile content did not significantly affect it.
5. BT-filled NBR composite demonstrated a higher dielectric constant of  $\sim 25$  and a lower dielectric loss of 0.15 at room temperature and frequency of  $10^5$  Hz compared to virgin NBR or CCTO-filled NBR composite. The dielectric constant decreased with acrylonitrile content. These composites have potential candidates in flexible dielectric materials.

**Acknowledgements** This research was financially supported by a grant from the government budget of Prince of Songkla University and Natural Rubber Innovation Research Institute (NR-IRI), contract no. SIT610284S, the graduate school of Prince of Songkla University, and by Prince of Songkla University, Surat Thani Campus. The authors would like to express their gratitude to the Faculty of Bioengineering and Technology, Universiti Malaysia Kelantan, for providing their facilities and equipment. We are grateful to Assoc. Prof. Dr. Seppo Karrila for his assistance with manuscript preparation.

## References

1. Caprarescu S, Radu AL, Purcar V, Sarbu A, Vaireanu DI, Ianchis R, Ghiurea M (2014) Removal of copper ions from simulated wastewaters using different bicomponent polymer membranes. *Water Air Soil Pollut* 225:2079 (1–12)
2. Simona C, Raluca I, Laura RA, Andrei S, Raluca S, Bogdan T, Elvira A, Ilie SC, Claudiu FR, Daniela IE, Silviu P, Ionut AL, Dan D (2017) Synthesis, characterization and efficiency of new organically modified montmorillonite polyethersulfone membranes for removal of zinc ions from wastewaters. *Appl Clay Sci* 137:135–142
3. Caprarescu S, Ion-Ebrasu D, Soare A, Purcar V, Radu AL, Sarbu A, Pascu M, Modrojan C, Dancila AM, Deleanu C (2019) Removal of nickel ions from synthetic wastewater using copolymers/natural extract blend membranes. *Rom J Phys* 64(821):1–10
4. Ion-Ebrasu D, Pollet BG, Spinu-Zaulet A, Soare A, Carcadea E, Varlam M, Caprarescu S (2019) Graphene modified fluorinated cation-exchange membranes for proton exchange membrane water electrolysis. *Int Hydrog Energy* 44:10190–10196
5. Atanase LI, Riess G (2013) Micellization of pH-stimulable poly(2-vinylpyridine)-b-poly(ethylene oxide) copolymers and their complexation with anionic surfactants. *J Colloid Interface Sci* 395:190–197

6. Gopinath S, Adarsh NN, Nair PR, Mathew S (2020) One-way thermo-responsive shape memory polymer nanocomposite derived from polycaprolactone and polystyrene-block-polybutadiene-block-polystyrene packed with carbon nanofiber. *Mater Today Commun* 22:1008022 (1–8)
7. Cui X, Chen J, Zhu Y, Jiang W (2020) Natural sunlight-actuated shape memory materials with reversible shape change and self-healing abilities based on carbon nanotubes filled conductive polymer composites. *Chem Eng J* 382:122823 (1–11)
8. Liu C, Li J, Jin Z, Hou P, Zhao H, Wang L (2019) Synthesis of graphene-epoxy nanocomposites with the capability to self-heal underwater for materials protection. *Compos Commun* 15:155–161
9. Chameswary J, Sebastian M (2015) Preparation and properties of BaTiO<sub>3</sub> filled butyl rubber composites for flexible electronic circuit applications. *J Mater Sci Mater* 26(7):4629–4637
10. Namitha L, Sebastian M (2017) High permittivity ceramics loaded silicone elastomer composites for flexible electronics applications. *Ceram Int* 43(3):2994–3003
11. Gu L, Li T, Xu Y, Sun C, Yang Z, Zhu D, Chen D (2019) Effects of the particle size of BaTiO<sub>3</sub> fillers on fabrication and dielectric properties of BaTiO<sub>3</sub>/polymer/Al films for capacitor energy-storage application. *Materials* 12(3):439 (1–16)
12. Zhu S, Guo J, Zhang J (2018) Enhancement of mechanical strength associated with interfacial tension between barium titanate and acrylonitrile-butadiene rubber with different acrylonitrile contents by surface modification. *J Appl Polym Sci* 135(9):45936 (1–10)
13. Ahmad H, Ismail H, Azura A (2015) Comparison properties of natural rubber/virgin acrylonitrile-butadiene rubber and natural rubber/recycled acrylonitrile-butadiene rubber blends. *Iran Polym J* 24:185–195
14. Whelan A, Lee K (2013) Developments in rubber technology—2: synthetic rubbers. In: Bertram HH (ed) *Developments in acrylonitrile-butadiene rubber (NBR) and future prospects*. Applied Science Publishers LTD, Essex, pp 51–52
15. El-Nemr KF (2011) Effect of different curing systems on the mechanical and physico-chemical properties of acrylonitrile butadiene rubber vulcanizates. *Mater Des* 32:3361–3369
16. Bokobza L (2018) Natural rubber nanocomposites: a review. *Nanomaterials* 9(1):12 (1–21)
17. Morsy R, Ismael M, Yehia A (2013) Conductivity studies on acrylonitrile butadiene rubber loaded with different types of carbon blacks. *Int J Mater Methods Technol* 1:22–35
18. Balachandran M, Bhagawan S (2012) Mechanical, thermal and transport properties of nitrile rubber (NBR)—nanoclay composites. *J Polym Res* 19:9809 (1–10)
19. Amin LMN, Ismail H, Nadras O (2018) Comparative study of bentonite filled acrylonitrile butadiene rubber and carbon black filled NBR composites properties. *Int J Auto Mech Eng* 15:5468–5479
20. Sadek E, El-Nashar D, Ahmed S (2018) Influence of modifying agents of organoclay on the properties of nanocomposites based on acrylonitrile butadiene rubber. *Egypt J Pet* 27:1177–1185
21. Kapgate BP, Das C, Basu D, Das A, Heinrich G (2015) Rubber composites based on silane-treated Stöber silica and nitrile rubber: interaction of treated silica with rubber matrix. *J Elastom Plast* 47:248–261
22. Eyssa H, Abulyazied D, Abdulrahman M, Youssef H (2018) Mechanical and physical properties of nanosilica/nitrile butadiene rubber composites cured by gamma irradiation. *Egypt J Pet* 27:383–392
23. Chaichan MT, Jawad RS, Hussein RM (2017) The influence of graphene oxide addition on the fortified nitrile butadiene rubber nano-composite qualities. *Al-Nahrain J Eng Sci* 20:904–910
24. Dief Allah M, Ali Z, Rozik NN, Raslan M, Sadek KU (2017) Electrical and mechanical properties of Nitrile rubber (NR) filled with industrial waste and by product from manufacture of ferrosilicon alloys in Egyptian chemical industries company. *Egypt J Chem* 60:905–918
25. Valentini L, Bon SB, Hernández M, López-Manchado MA, Pugno N (2018) Nitrile butadiene rubber composites reinforced with reduced graphene oxide and carbon nanotubes show superior mechanical, electrical and icephobic properties. *Compos Sci Technol* 166:109–114
26. Pingot M, Szadkowski B, Zaborski M (2018) Effect of carbon nanofibers on mechanical and electrical behaviors of acrylonitrile-butadiene rubber composites. *Polym Adv Technol* 29:1661–1669
27. Su J, Zhang J (2016) Reinforced properties of ethylene-propylene-diene monomer composites by vinyltrimethoxysiloxane functionalised barium titanate. *Plast Rubber Compos* 45:127–135
28. Šupová M, Martynková GS, Barabaszová K (2011) Effect of nanofillers dispersion in polymer matrices: a review. *Sci Adv Mater* 3:1–25
29. Luo B, Wang X, Zhao Q, Li L (2015) Synthesis, characterization and dielectric properties of surface functionalized ferroelectric ceramic/epoxy resin composites with high dielectric permittivity. *Compos Sci Technol* 112:1–7

30. Li L, Zheng S (2016) Enhancement of dielectric constants of epoxy thermosets via a fine dispersion of barium titanate nanoparticles. *J Appl Polym Sci* 133:43322 (1–10)
31. Gonzalez N, Tomara GN, Psarras GC, Riba JR, Armelin E (2017) Dielectric response of vulcanized natural rubber containing BaTiO<sub>3</sub> filler: the role of particle functionalization. *Eur Polym J* 97:57–67
32. Guan S, Li H, Zhao S, Guo L (2018) The surface modification of BaTiO<sub>3</sub> and its effects on the microstructure and electrical properties of BaTiO<sub>3</sub>/silicone rubber composites. *J Vinyl Addit Technol* 24:288–294
33. Zhang X, Wang Y, Sheng Y, Ye H, Xu L, Wu H (2019) Enhanced energy density in hydroxyl-modified barium titanate/poly (fluorovinylidene-co-trifluoroethylene) nanocomposites with improved interfacial polarization. *Chem Phys Lett* 723:89–95
34. Hamciuc E, Hamciuc C, Bacosca I, Cristea M, Okrasa L (2011) Thermal and electrical properties of nitrile-containing polyimide/BaTiO<sub>3</sub> composite films. *Polym Compos* 32:846–855
35. Phan TTM, Chu NC, Luu VB, Xuan HN, Pham DT, Martin I, Carrière P (2016) Enhancement of polarization property of silane-modified BaTiO<sub>3</sub> nanoparticles and its effect in increasing dielectric property of epoxy/BaTiO<sub>3</sub> nanocomposites. *J Sci Adv Mater Dev* 1:90–97
36. Zhu S, Zhang J (2017) Enhanced dielectric constant of acrylonitrile–butadiene rubber/barium titanate composites with mechanical reinforcement by nanosilica. *Iran Polym J* 26:239–325
37. Saidina D, Mariatti M, Julie M (2014) Properties of calcium copper titanate and barium titanate filled epoxy composites for electronic applications: effect of filler loading and hybrid fillers. *J Mater Sci Mater Electron* 25:4923–4932
38. Dang ZM, Zhou T, Yao SH, Yuan JK, Zha JW, Song HT, Li JY, Chen Q, Yang WT, Bai J (2009) Advanced calcium copper titanate/polyimide functional hybrid films with high dielectric permittivity. *Adv Mater* 21:2077–2082
39. Yang W, Yu S, Sun R, Du R (2011) Nano-and microsize effect of CCTO fillers on the dielectric behavior of CCTO/PVDF composites. *Acta Mater* 59:5593–5602
40. Chi Q, Sun J, Zhang C, Liu G, Lin J, Wang Y, Wang X, Lei Q (2014) Enhanced dielectric performance of amorphous calcium copper titanate/polyimide hybrid film. *J Mater Chem C* 2:172–177
41. Romasanta LJ, Leret P, Casaban L, Hernández M, Miguel A, Fernández JF, Kenny JM, Lopez-Manchado MA, Verdejo R (2012) Towards materials with enhanced electro-mechanical response: CaCu<sub>3</sub>Ti<sub>4</sub>O<sub>12</sub>-polydimethylsiloxane composites. *J Mater Chem* 22:24705–24712
42. Wang GL, Zhang YY, Duan L, Ding KH, Wang ZF, Zhang M (2015) Property reinforcement of silicone dielectric elastomers filled with self-prepared calcium copper titanate particles. *J Appl Polym Sci* 132:42613 (1–6)
43. Duan L, Wang GL, Zhang YY, Zhang YN, Wei YY, Wang ZF, Zhang M (2018) High dielectric and actuated properties of silicone dielectric elastomers filled with magnesium-doped calcium copper titanate particles. *Polym Compos* 39:691–697
44. Singh AP, Singh Y (2016) Dielectric behavior of CaCu<sub>3</sub>Ti<sub>4</sub>O<sub>12</sub>: Polyvinyl chloride ceramic polymer composites at different temperature and frequencies. *Mod Electron Mater* 2:121–126
45. Xie C, Liang F, Ma M, Chen X, Lu W, Jia Y (2017) Microstructure and dielectric properties of PTFE-based composites filled by micron/submicron-blended CCTO. *Crystals* 7(5):126 (1–8)
46. Yang J, Tang Z, Yin H, Liu Y, Wang L, Tang H, Li Y (2019) Poly (arylene ether nitrile) composites with surface-hydroxylated calcium copper titanate particles for High-temperature-resistant dielectric applications. *Polymers* 11(5):766 (1–11)
47. Rodgers B (2015) Rubber compounding: chemistry and applications. In: Hoover FI, To BH (eds) *Vulcanization*, 2nd edn. CRC Press, Florida, p 464
48. Choi SS (2001) Improvement of properties of silica-filled styrene–butadiene rubber compounds using acrylonitrile–butadiene rubber. *J Appl Polym Sci* 79:1127–1133
49. Chokanandsombat Y, Owjinda S, Sirisinha C (2012) Comparison on properties of acrylonitrile styrene butadiene rubber (NSBR) and styrene butadiene rubber (SBR)/nitrile rubber (NBR) blends. *KGK* 11(12):41–46
50. Ismail H, Ramly A, Othman N (2011) The effect of carbon black/multiwall carbon nanotube hybrid fillers on the properties of natural rubber nanocomposites. *Polym Plast Technol Eng* 50:660–666
51. Ismail H, Ishak S, Hamid Z (2013) Comparison effect of mica and talc as filler in EPDM composites on curing, tensile and thermal properties. *Prog Rubber Plast Re* 29:109–122
52. Dang ZM, Lin YQ, Xu HP, Shi CY, Li ST, Bai J (2008) Fabrication and dielectric characterization of advanced BaTiO<sub>3</sub>/polyimide nanocomposite films with high thermal stability. *Adv Funct Mater* 18:1509–1517

53. Salaeh S, Muensit N, Bomlai P, Nakason C (2011) Ceramic/natural rubber composites: influence types of rubber and ceramic materials on curing, mechanical, morphological, and dielectric properties. *J Mater Sci* 46:1723–1731
54. Yuan X, Shen F, Wu G, Wu C (2007) Effects of acrylonitrile content on the coordination crosslinking reaction between acrylonitrile–butadiene rubber and copper sulfate. *Mater Sci Eng C* 459:82–85
55. Song M, Zhao X, Li Y, Chan TW, Zhang L, Wu S (2014) Effect of acrylonitrile content on compatibility and damping properties of hindered phenol AO-60/nitrile-butadiene rubber composites: Molecular dynamics simulation. *RSC Adv* 4:48472–48479
56. Thipdech P, Kunanurksapong R, Sirivat A (2008) Electromechanical responses of poly(3-thiopheneacetic acid)/acrylonitrile-butadiene rubbers. *Express Polym Lett* 2(12):866–877
57. Abd-El Messieh SL, Rozik NN, Youssef NF (2019) Eco-friendly composites based on ceramic tiles industrial wastes and acrylonitrile butadiene rubber. *Polym Compos* 40:544–552
58. George S, Varughese K, Thomas S (1999) Dielectric properties of isotactic polypropylene/nitrile rubber blends: Effects of blend ratio, filler addition, and dynamic vulcanization. *J Appl Polym Sci* 73:255–270

**Publisher's Note** Springer Nature remains neutral with regard to jurisdictional claims in published maps and institutional affiliations.